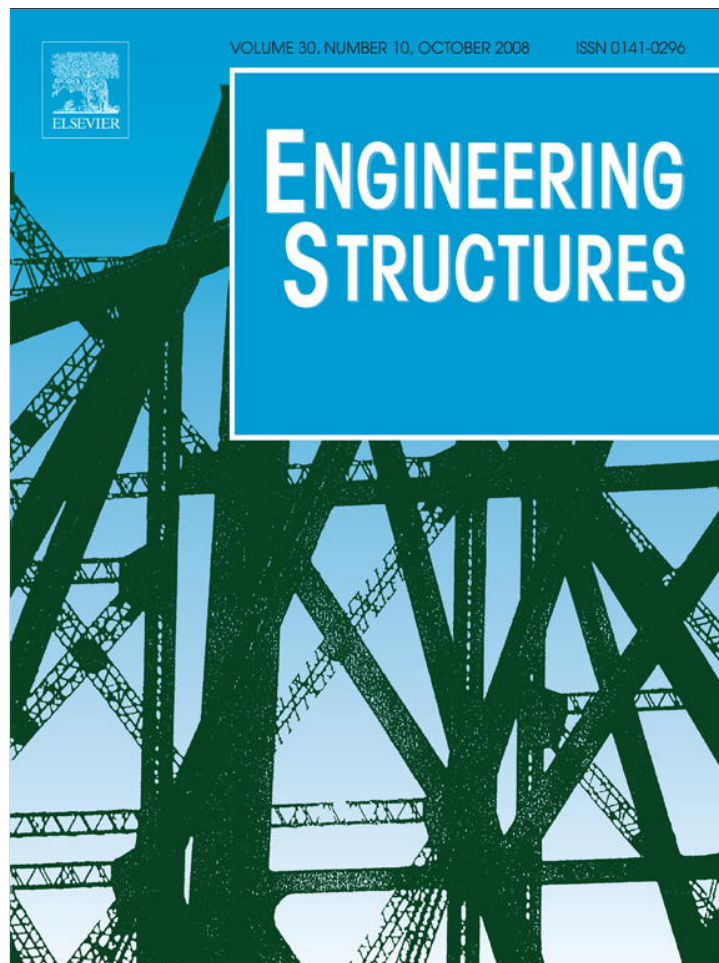


Provided for non-commercial research and education use.
Not for reproduction, distribution or commercial use.



This article appeared in a journal published by Elsevier. The attached copy is furnished to the author for internal non-commercial research and education use, including for instruction at the authors institution and sharing with colleagues.

Other uses, including reproduction and distribution, or selling or licensing copies, or posting to personal, institutional or third party websites are prohibited.

In most cases authors are permitted to post their version of the article (e.g. in Word or Tex form) to their personal website or institutional repository. Authors requiring further information regarding Elsevier's archiving and manuscript policies are encouraged to visit:

<http://www.elsevier.com/copyright>



ELSEVIER

Available online at www.sciencedirect.com

Engineering Structures 30 (2008) 2631–2643

**ENGINEERING
STRUCTURES**

www.elsevier.com/locate/engstruct

Elastic postbuckling stiffness of biaxially compressed rectangular plates

Eivind Steen^{a,*}, Eirik Byklum^a, Jostein Helleland^b

^a *Det Norske Veritas AS, DNV Maritime, Veritasvn. 1, NO-1322 Høvik, Norway*

^b *University of Oslo, Department of Mathematics, Mechanics Division, NO-0316 Oslo, Norway*

Received 28 June 2007; received in revised form 4 February 2008; accepted 8 February 2008

Available online 14 April 2008

Abstract

The elastic buckling and postbuckling response of biaxially compressed plates is analysed with main focus on change of in-plane postbuckling stiffness under prescribed plate shortenings rather than the more normal load control. An analytical closed-form single-degree-of-freedom solution is derived and compared with an analytical multi-degree-of-freedom model. Results for the analytical multi-degree-of-freedom-model are obtained by solving numerically the equilibrium equations using the perturbation expansion technique with arc length control in an incremental scheme. Both models are applied to specific plate examples and comparisons with results obtained using a commercial nonlinear finite element program are included.

© 2008 Elsevier Ltd. All rights reserved.

Keywords: Thin plates; Postbuckling stiffness; Large deflections; Semi-analytical; Combined loads

1. Introduction

It is well known that the membrane (in-plane) stiffness of thin plates drops as they are compressed beyond their elastic buckling limit and into the postbuckling region. Many studies on these effects have been presented in the literature over the last three decades, but far from all characteristics of the geometrical nonlinear plate responses are explored. One area that is not documented in any detail is the postbuckling response of biaxially compressed plates under plate-edge-shortening control rather than the normally assumed load control. Since the edge-shortening (displacement) control is most realistic for plates being part of larger structures, this topic is of practical interest in general and in a design code context in particular.

Publication of results on the topic of buckling and postbuckling behaviour of plates has been extensive over the last three decades. Some of the pioneers addressing the theoretical aspects of the problem are Koiter [1,2], Budiansky [3] and Tvergaard [4]. A short selection of more practical engineering publications are [5–11]. Steen [12–14] addressed the stiffness change of elastically buckled plates and developed closed-form solutions and numerical schemes suited for simplified, semi-analytical stiffened plate buckling models.

Byklum et al. [15–18] extended this theory and developed semi-analytical, multi-degree-of-freedom models suited for ultimate strength and stiffness assessment of stiffened as well as unstiffened plates. These models have been implemented and constitute the basis for a computerized buckling assessment code called PULS (Panel Ultimate Limit State) [19]. This code is commercially available and recognized by Det Norske Veritas [20] and other third party institutions and it is used by designers and consultants world wide.

The purpose of the present paper is to study the postbuckling behaviour of plates subjected to biaxial plate-edge-shortening control and to trace the resulting biaxial load redistribution and the corresponding postbuckling stiffness. Since normal design procedures do not distinguish between load and plate-shortening control, it is of interests to highlight this difference and to assess the consequences. This will lead to an improved understanding of the mechanics involved and hopefully build a basis for more realistic and accurate design procedures in the future. Moreover, as the load-shortening response of individual plate elements embrace the load- and plate-shortening characteristics into a single consistent relation, the present models may constitute a sound foundation for developing macro-material models applicable for global ultimate strength analysis of ship hulls etc. in which geometrical as well as material nonlinearities are dealt with.

Two analytical models, dealing with the nonlinear geometrical effect, are described in the present paper. The first is an

* Corresponding author.

E-mail address: Eivind.Steen@dnv.com (E. Steen).

analytical, single-degree-of-freedom (SDOF), closed-form solution presented by Steen [13]. The second is a more advanced analytical, multi-degree-of-freedom-model (MDOF) presented by Byklum [17], but here transformed to a form appropriate for plate-shortening control. Results from the two models for some specific plate examples are compared with corresponding results obtained using a commercial finite element program [21].

2. Macro-material concepts — load-shortening curves

In simplified global nonlinear strength analysis of ship hulls and other large plated structures, it is desired to represent the load-shortening response characteristics of individual plates in a computationally efficient manner. The concept is to model local plated areas relatively coarse and to lump all nonlinear geometrical and material effects into the corresponding “macro-material” element characteristics. This idea has been pursued by many researchers over the last decades and a lot of different approaches and results have been published, e.g. [22–24]. An overview of some of these approaches can be found in Paik and Thayamballi [25]. Despite the appealing simplicity of the method, it has not yet reached a level where all important effects required for practical applications to ship hulls are included. But by continuous efforts in developing more rigorous macro-models on the local level, it is believed that the method will be part of engineering design procedures some years ahead.

The general macro-material model should cover the simultaneous action of in-plane biaxial and shear loads acting on a buckled rectangular plate, Fig. 1. Mathematically the macro-model valid for any equilibrium state relates acting in-plane loads $\sigma_1, \sigma_2, \sigma_3$ (per unit area or per unit plate length) and the corresponding in-plane shortenings $\varepsilon_1, \varepsilon_2, \varepsilon_3$ may formally be written as

$$\sigma_\alpha = \sigma_\alpha(\varepsilon_1, \varepsilon_2, \varepsilon_3) \quad \alpha = 1, 2, 3 \quad (1)$$

The general tensor notation is used for convenience, with the subscript 1 and 2 indicating the in-plane axial and transverse directions respectively and subscript 3 the in-plane shear direction.

The term of pseudo- or macro-material element characteristics is natural since the format hides the out-of-plane buckling displacements and directly gives a mathematical relationship between stresses and strains. An alternative and much used terminology for the same is load shortening or average stress–strain curves. The latter notions have been commonly used for stiffened panels subjected to uniaxial loading only.

By expanding Eq. (1) around a known state I_s , the material model is transformed to the incremental form defined by

$$\Delta\sigma_\alpha = C_{\alpha\beta}\Delta\varepsilon_\beta + C_{\alpha\beta\delta}\Delta\varepsilon_\beta\Delta\varepsilon_\delta + \dots \quad \alpha, \beta, \delta = 1, 2, 3 \quad (2)$$

where the macro-material coefficients are defined by

$$C_{\alpha\beta} \equiv \frac{\partial\sigma_\alpha}{\partial\varepsilon_\beta} \quad (3)$$

$$C_{\alpha\beta\delta} \equiv \frac{1}{2!} \frac{\partial^2\sigma_\alpha}{\partial\varepsilon_\beta\partial\varepsilon_\delta} \quad \alpha, \beta, \delta = 1, 2, 3$$

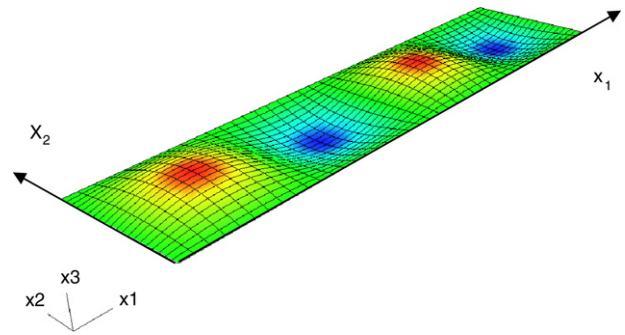


Fig. 1. Buckled rectangular plate.

In order to better illustrate the various first-order term coefficients, i.e. the tangential stiffness coefficients $C_{\alpha\beta}$, Eq. (2) can be rewritten on matrix form as follows:

$$\begin{bmatrix} \Delta\sigma_1 \\ \Delta\sigma_2 \\ \Delta\sigma_3 \end{bmatrix} = \begin{bmatrix} C_{11} & C_{12} & C_{13} \\ C_{21} & C_{22} & C_{23} \\ C_{31} & C_{32} & C_{33} \end{bmatrix} \begin{bmatrix} \Delta\varepsilon_1 \\ \Delta\varepsilon_2 \\ \Delta\varepsilon_3 \end{bmatrix} + \text{higher-order} \quad (4)$$

Analogous with the deformation theory of plasticity [26], Eq. (1) can be interpreted as a nonlinear macro-material model on total form. Similarly, Eq. (2) or (4), with only the first-order terms included, represent the analogy to the incremental flow theory of plasticity.

The stiffness coefficients are state dependent and will typically have values close to the linear elastic ones for small loads and gradually decrease as the loading and the out-of-plane deflections increase, in particularly close to and beyond the elastic buckling level.

The important feature of this macro-model is that the incremental stresses and strains referred to are not at a material point, but rather represent the acting loads (average stresses) and the corresponding relative plate shortenings (average strains) of the considered plate field. This is important to note when employing the present macro-material model in a nonlinear finite element method (FEM) program. Typical optimal mesh density (element size) will be one element between longitudinal stiffeners.

In the case of only two independent loads, Eq. (1) is reduced to the two equilibrium surfaces defined by

$$\begin{aligned} \sigma_1 &= \sigma_1(\varepsilon_1, \varepsilon_2) \\ \sigma_2 &= \sigma_2(\varepsilon_1, \varepsilon_2) \end{aligned} \quad (5)$$

This case is easier to illustrate graphically. In the three-dimensional space spanned by $(\sigma_\alpha, \varepsilon_1, \varepsilon_2)$, these functions can be shown as two-dimensional surfaces. Mapped into the two-dimensional strain space $(\varepsilon_1, \varepsilon_2)$, one surface is schematically illustrated in Fig. 2 as a set of $\sigma_\alpha = \text{constant}$ contour curves. The gradient $\nabla\sigma_\alpha$ to these surfaces is the vector

$$\nabla\sigma_\alpha = C_{\alpha 1}\mathbf{i}_1 + C_{\alpha 2}\mathbf{i}_2 \quad (6)$$

It is directed normal to the contour curves and gives the direction along which the maximum stiffness is achieved.

A loaded plate will follow a load history path across this equilibrium surface as indicated by example curves 1 and 2 emanating from origin. For the simplest case of proportional

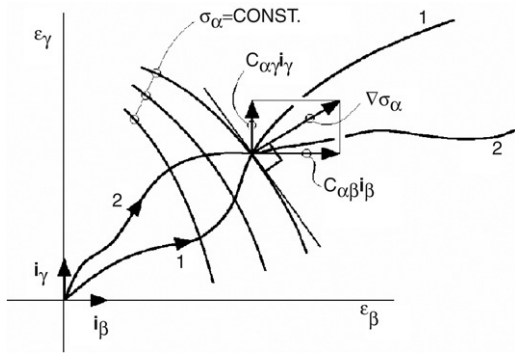


Fig. 2. Schematic illustration of load-shortening contour curves of a biaxially loaded plate.

load paths in strain space, the load history is defined by the unit tangent vector

$$\mathbf{t}_d = \varepsilon_1(t)\mathbf{i}_1 + \varepsilon_2(t)\mathbf{i}_2 = \cos d\mathbf{i}_1 + \sin d\mathbf{i}_2 \quad (7)$$

Here the proportional load history angle d is measured from the positive ε_1 strain axis. The directional stiffness along this tangent \mathbf{t}_d for any load component σ_α is thus given by the scalar product

$$C_\alpha^d \equiv \nabla\sigma_\alpha \cdot \mathbf{t}_d \quad \alpha = 1, 2 \quad (8)$$

As an example, the directional stiffness for the axial stress σ_1 of a biaxially loaded plate is simply

$$\begin{aligned} C_1^d &= \nabla\sigma_1 \cdot \mathbf{t}_d \\ C_1^d &= C_{11} \cos d + C_{12} \sin d \end{aligned} \quad (9)$$

Closed-form solutions for the directional stiffness are given for some examples in Eqs. (46)–(48).

3. Closed-form solution (SDOF)

3.1. Derivations

For the general problem of simultaneous biaxial compression and shear acting on a rectangular plate, the buckling and postbuckling pattern will be very complex. For such a problem, multi-degrees-of-freedom-models will be required to describe the correct physical behaviour [15,18]. However, for the important case of biaxial loading, which is considered below, the nonlinear geometrical behaviour can be analysed reasonably accurate with only a single-degree-of-freedom (SDOF), at least as long as the plate aspect ratio of the buckling pattern is not too large and the plate slenderness is not too high.

The internal membrane stresses in a deformed plate can be found by solving Marguerre's compatibility equation [26,27], which for an isotropic plate with imperfections takes the form

$$\begin{aligned} \nabla^4 F &= E[w_{,12}^2 - w_{,11}w_{,22} \\ &+ 2w_{0,12}w_{,12} - w_{0,11}w_{,22} - w_{0,22}w_{,11}] \end{aligned} \quad (10)$$

The basis for the derivation of Eq. (10) are Marguerre's kinematic relations defined as

$$\begin{aligned} \varepsilon_{11} &= u_{1,1} + \frac{1}{2}w_{,1}^2 + w_{,1}w_{0,1} \\ \varepsilon_{22} &= u_{2,2} + \frac{1}{2}w_{,2}^2 + w_{,2}w_{0,2} \\ \varepsilon_{12} &= \frac{1}{2}(u_{1,2} + u_{2,1}) + \frac{1}{2}(w_{,1}w_{,2} + w_{,1}w_{0,2} + w_{,2}w_{0,1}) \end{aligned} \quad (11)$$

In Eq. (10), F denotes Airy's stress function, w is the lateral deflection due to the applied loads added on top of the stress-free initial lateral imperfection w_0 . The u_1 and u_2 represent the in-plane displacement in the x_1 and x_2 direction, respectively. A comma followed by a subscript 1 denotes partial derivative with respect to coordinate x_1 etc.

Assuming the buckling and initial imperfection pattern to be in the same form with one single Fourier term, the lateral displacements w and w_0 for a plate with length a and width b is expressed by

$$\begin{aligned} w &= q_1 t \sin\left(\frac{m\pi}{a}x_1\right) \sin\left(\frac{n\pi}{b}x_2\right) \\ w_0 &= q_{10} t \sin\left(\frac{m\pi}{a}x_1\right) \sin\left(\frac{n\pi}{b}x_2\right) \end{aligned} \quad (12)$$

The coefficients q_1 and q_{10} are deflection parameters non-dimensionalized with respect to the plate thickness t , and defined by

$$q_1 = \frac{A_{mn}}{t}, \quad q_{10} = \frac{A_{mn}^0}{t} \quad (13)$$

Here, A_{mn} and A_{mn}^0 are the Fourier amplitudes for the load dependent and stress-free imperfection displacements, respectively. The corresponding deflection pattern has m half-waves in the x_1 direction and n half-waves in the x_2 direction.

The set of integers (m, n) determines the shape of the buckling mode, and the actual values to be used in a given case can be varied to study different effects. The normal procedure is to use the set (m, n) that minimizes the eigenvalue.

With the assumed displacements, Eq. (12), the solution of the compatibility equation, Eq. (10), gives the following solution for the internal redistributed membrane stresses:

$$\begin{aligned} \sigma_{11} &= -\sigma_1 - \frac{\pi^2 E}{8}(2q_{10}q_1 + q_1^2) \left[\left(\frac{tm}{a}\right)^2 \cos\frac{2n\pi}{b}x_2 \right] \\ \sigma_{22} &= -\sigma_2 - \frac{\pi^2 E}{8}(2q_{10}q_1 + q_1^2) \left[\left(\frac{tn}{b}\right)^2 \cos\frac{2m\pi}{a}x_1 \right] \\ \sigma_{12} &= 0. \end{aligned} \quad (14)$$

The membrane stress distribution of Eq. (10) implies straight in-plane plate edges.

The adopted sign convention defines the external stresses (σ_1, σ_2) and the corresponding relative plate shortenings $(\varepsilon_1, \varepsilon_2)$ as positive in compression. On the other hand, internal membrane stress $\sigma_{\alpha\beta}$; $\alpha, \beta = 1, 2$ and corresponding strains $\varepsilon_{\alpha\beta}$ are defined, as usual, as positive in tension.

Using Hooke's law for plane stress, the internal membrane stresses are transformed to membrane strains as

$$\begin{aligned} \varepsilon_{11} &= -\frac{1}{E}(\sigma_1 - \nu\sigma_2) - \frac{\pi^2}{8}(2q_{10}q_1 + q_1^2) \\ &\quad \times \left[\left(\frac{tm}{a}\right)^2 \cos \frac{2n\pi}{b}x_2 - \nu \left(\frac{tn}{b}\right)^2 \cos \frac{2m\pi}{a}x_1 \right] \\ \varepsilon_{22} &= -\frac{1}{E}(\sigma_2 - \nu\sigma_1) - \frac{\pi^2}{8}(2q_{10}q_1 + q_1^2) \\ &\quad \times \left[\left(\frac{tn}{b}\right)^2 \cos \frac{2m\pi}{a}x_1 - \nu \left(\frac{tm}{a}\right)^2 \cos \frac{2n\pi}{b}x_2 \right] \end{aligned} \quad (15)$$

$$\varepsilon_{12} = 0$$

By defining the relative plate shortenings as

$$\begin{aligned} \varepsilon_1 &\equiv \frac{1}{ab} \int u_{1,1} dA \\ \varepsilon_2 &\equiv \frac{1}{ab} \int u_{2,2} dA \end{aligned} \quad (16)$$

and using the kinematic relations in Eq. (11), and Eqs. (13) and (15), the plate shortenings can be expressed as

$$\begin{aligned} \varepsilon_1 &= \frac{1}{E}(\sigma_1 - \nu\sigma_2) + \frac{\pi^2}{8}(2q_{10}q_1 + q_1^2) \left(\frac{tm}{a}\right)^2 \\ \varepsilon_2 &= \frac{1}{E}(\sigma_2 - \nu\sigma_1) + \frac{\pi^2}{8}(2q_{10}q_1 + q_1^2) \left(\frac{tn}{b}\right)^2 \end{aligned} \quad (17)$$

This is the macro-model on total form for the shortening-load relationship. Inverted it gives the following load-shortening relationship:

$$\begin{aligned} \sigma_1 &= \frac{E}{1-\nu^2}(\varepsilon_1 + \nu\varepsilon_2) - \frac{\pi^2}{8} \frac{E}{1-\nu^2} \\ &\quad \times (q_1^2 + 2q_{10}q_1)(k_1 + \nu k_2) \\ \sigma_2 &= \frac{E}{1-\nu^2}(\varepsilon_2 + \nu\varepsilon_1) - \frac{\pi^2}{8} \frac{E}{1-\nu^2} \\ &\quad \times (q_1^2 + 2q_{10}q_1)(k_2 + \nu k_1) \end{aligned} \quad (18)$$

where k_1 and k_2 are constants defined by Eq. (21).

Applying the classical thin-walled plate theory of Kirchhoff [26,28], the potential energy of a rectangular plate subjected to uniform biaxial loads (σ_1, σ_2), shear (τ) and lateral pressure p can be expressed as

$$\begin{aligned} V &= \frac{Et^3}{24(1-\nu^2)} \\ &\quad \times \int [w_{,11}^2 + w_{,22}^2 + 2\nu w_{,11}w_{,22} + 2(1-\nu)w_{,12}^2] dA \\ &\quad + \frac{t}{2E} \int [(\sigma_{11} + \sigma_{22})^2 - 2(1+\nu)(\sigma_{11}\sigma_{22} - (\sigma_{12})^2)] dA \\ &\quad - t\sigma_1 \int u_{1,1} dA - t\sigma_2 \int u_{2,2} dA \\ &\quad - t\tau \int (u_{1,2} + u_{2,1}) dA - p \int w dA \end{aligned} \quad (19)$$

The area integration is taken over a plate with length a and width b .

In the remainder of this section, we will limit the presentation to the case of in-plane, biaxial loading only, which is the loading of main interest here. However, in principle, the other effects can readily be included in the formulations.

By substituting Eqs. (15)–(17) into Eq. (5), the final expression for the potential energy V for a plate subjected to biaxial loading becomes

$$\begin{aligned} V &= \frac{\pi^4}{256} E(2q_1q_{10} + q_1^2)^2(k_1^2 + k_2^2) \\ &\quad + \frac{\pi^4}{96(1-\nu^2)} E q_1^2(k_1 + k_2)^2 \\ &\quad - \frac{\pi^2}{8}(2q_1q_{10} + q_1^2)(k_1\sigma_1 + k_2\sigma_2) \end{aligned} \quad (20)$$

where per definition

$$k_1 = \left(\frac{t}{\ell_1}\right)^2, \quad k_2 = \left(\frac{t}{\ell_2}\right)^2, \quad \ell_1 = \frac{a}{m}, \quad \ell_2 = \frac{b}{n} \quad (21)$$

The nonlinear equilibrium equation is derived from the principle of stationary potential energy, i.e.

$$f_1(q_1, \sigma_1, \sigma_2) \equiv \frac{\partial V}{\partial q_1} = 0 \quad (22)$$

This yields

$$\begin{aligned} f_1 &\equiv \frac{\pi^4}{64} E(2q_1q_{10} + q_1^2)(q_1 + q_{10})(k_1^2 + k_2^2) \\ &\quad + \frac{\pi^4}{48(1-\nu^2)} E q_1(k_1 + k_2)^2 \\ &\quad - \frac{\pi^2}{4}(q_{10} + q_1)(k_1\sigma_1 + k_2\sigma_2) = 0 \end{aligned} \quad (23)$$

This equilibrium equation is expressed in terms of the in-plane loads σ_1, σ_2 . Thus it is suited for studying the plate response under load control, i.e. the load history has to be defined in load space (σ_1, σ_2).

In order to study the plate response in the end-shortening space ($\varepsilon_1, \varepsilon_2$), the loads have to be transformed to plate shortenings using Eq. (18).

3.2. Closed-form equilibrium solution

In the following, the equilibrium solution, Eq. (23), for the biaxial, in-plane loading case is written in a compact closed-form for both load control and plate-shortening control.

3.2.1. Load control

Eq. (23) can be transformed to the simple form given by

$$A_\sigma = \frac{q_1}{q_1 + q_{10}}(1 + a_2(q_1^2 + 3q_1q_{10} + 2q_{10}^2)) \quad (24)$$

where

$$A_\sigma = \frac{12(1-\nu^2)}{\pi^2 E} \left(\frac{\ell_2}{t}\right)^2 \frac{((\ell_2/\ell_1)^2\sigma_1 + \sigma_2)}{(1 + (\ell_2/\ell_1)^2)^2} \quad (25)$$

$$a_2 = \frac{3}{4}(1-\nu^2) \frac{1 + (\ell_2/\ell_1)^4}{(1 + (\ell_2/\ell_1)^2)^2} \quad (26)$$

Λ_σ is a non-dimensional load parameter, representing the combined load effect. It takes the value of unity at the elastic buckling level (eigenvalues). The a_2 parameter is the classical Koiter postbuckling coefficient representing the curvature of the postbuckling path at the elastic buckling level.

3.2.2. Plate-shortening control

By replacing the loads by plate shortenings, using Eq. (19), the equilibrium equation can be written as

$$\Lambda_\varepsilon = \frac{q_1}{q_1 + q_{10}} (1 + b_2(q_1^2 + 3q_1q_{10} + 2q_{10}^2)) \quad (27)$$

where

$$\Lambda_\varepsilon = \frac{12}{\pi^2} \left(\frac{\ell_2}{t} \right)^2 \frac{((\ell_2/\ell_1)^2 + \nu)\varepsilon_1 + (\nu(\ell_2/\ell_1)^2 + 1)\varepsilon_2}{(1 + (\ell_2/\ell_1)^2)^2} \quad (28)$$

$$b_2 = \frac{3(3 - \nu^2)(1 + (\ell_2/\ell_1)^4) + 12\nu(\ell_2/\ell_1)^2}{4(1 + (\ell_2/\ell_1)^2)^2} \quad (29)$$

Λ_ε is a non-dimensional load parameter, representing the combined plate-shortening effect. It takes the value of unity at the elastic buckling level (eigenvalues). The b_2 parameter is the classical postbuckling coefficient representing the curvature of the postbuckling path at the elastic buckling level.

Traditionally the equilibrium equation is given on a load control form. For comparison, the well-known Koiter theory [29] gives the equilibrium equation in the following form

$$\Lambda_\sigma = \frac{q_1}{q_1 + q_{10}} (1 + a_2q_1^2) \quad (30)$$

It is seen that the present closed-form solution (Eq. (24)) is very similar to the Koiter equation apart from two terms coupled to the initial imperfection amplitude q_{10} . For small imperfection amplitudes the two solutions converge. The Koiter solution is asymptotic in the sense that it is only valid for very small imperfections, while the present solution treats the nonlinear membrane effects more realistically for plates with medium and larger imperfection levels.

3.2.3. Eigenvalue solution

In later presentations of results, elastic buckling values (eigenvalues) will be included. As mentioned above, these can be obtained by setting Λ_σ and Λ_ε equal to unity. For $\Lambda_\sigma = 1$, Eq. (25) can be rewritten in a familiar and standard form as

$$\left(m^2\sigma_1 + \left(\frac{a}{b} \right)^2 n^2\sigma_2 \right) = \frac{\pi^2 E}{12(1 - \nu^2)} \left(\frac{t}{b} \right)^2 \left(\frac{b}{a} \right)^2 \times (m^2 + (a/b)^2 n^2)^2 \quad (31)$$

which, for a given buckling mode, represented by given integers m and n , will be represented by straight lines in the load space. The same will be the case for eigenvalue presentations in the plate-shortening space. For this case, Eq. (28) with $\Lambda_\varepsilon = 1$ can be rewritten as

$$\left(m^2 + \left(\frac{a}{b} \right)^2 n^2\nu \right) \varepsilon_1 + \left(\nu m^2 + \left(\frac{a}{b} \right)^2 n^2 \right) \varepsilon_2$$

$$= \frac{\pi^2}{12} \left(\frac{t}{b} \right)^2 \left(\frac{b}{a} \right)^2 (m^2 + (a/b)^2 n^2)^2 \quad (32)$$

3.3. Closed-form stiffness solution

For the biaxially loaded plate, the incremental macro-material model, Eq. (4) takes the following simple form

$$\begin{bmatrix} \Delta\sigma_1 \\ \Delta\sigma_2 \end{bmatrix} = \begin{bmatrix} C_{11} & C_{12} \\ C_{21} & C_{22} \end{bmatrix} \begin{bmatrix} \Delta\varepsilon_1 \\ \Delta\varepsilon_2 \end{bmatrix} \quad (33)$$

For conservative loading, such as considered in this paper, the stiffness matrix is symmetrical.

From the definition of the stiffness coefficients, Eq. (3), and by making use of Eq. (18), the following expressions emerge

$$\begin{aligned} C_{11} &= \frac{E}{1 - \nu^2} \left[1 - \frac{\pi^2}{4} (k_1 + \nu k_2)(q_1 + q_{10}) \frac{\partial q_1}{\partial \varepsilon_1} \right] \\ C_{12} &= \frac{E\nu}{1 - \nu^2} \left[1 - \frac{\pi^2}{4} (k_1 + \nu k_2)(q_1 + q_{10}) \frac{\partial q_1}{\partial \varepsilon_2} \right] = C_{21} \\ C_{22} &= \frac{E}{1 - \nu^2} \left[1 - \frac{\pi^2}{4} (k_2 + \nu k_1)(q_1 + q_{10}) \frac{\partial q_1}{\partial \varepsilon_2} \right] \end{aligned} \quad (34)$$

The derivatives of the deflection parameter are found from the equilibrium equation, Eq. (27), and can be written

$$\frac{\partial q_1}{\partial \varepsilon_\alpha} = \frac{(q_1 + q_{10})(\partial \Lambda_\varepsilon / \partial \varepsilon_\alpha)_\varepsilon}{1 + b_2(3q_1^2 + 6q_1q_{10} + 2q_{10}^2) - \Lambda_\varepsilon} \quad \alpha = 1, 2 \quad (35)$$

The derivative of the plate-shortening parameter in the denominator of this equation can readily be obtained from Eq. (28).

The stiffness coefficients given by Eq. (34) are valid for any equilibrium state for prescribed values of the deflection coefficient q_1 , the initial stress-free imperfection q_{10} and loaded state defined by either the plate shortenings ($\varepsilon_1, \varepsilon_2$) or physical loads (σ_1, σ_2).

From Eqs. (34) and (35) it can be shown that the values for the initial stiffness coefficients at zero load simplify

$$\begin{aligned} C_{11} &= \frac{E}{1 - \nu^2} \left[1 - 6 \frac{(k_1 + \nu k_2)^2}{A} \right] \\ C_{12} &= \frac{E\nu}{1 - \nu^2} \left[1 - \frac{6}{\nu} \frac{(k_1 + \nu k_2)(k_2 + \nu k_1)}{A} \right] = C_{21} \\ C_{22} &= \frac{E}{1 - \nu^2} \left[1 - 6 \frac{(k_2 + \nu k_1)^2}{A} \right] \end{aligned} \quad (36)$$

where the coefficient A is given by

$$A \equiv \frac{2(k_1 + k_2)^2}{q_{10}^2} + 3(3 - \nu^2)(k_1^2 + k_2^2) + 12\nu k_1 k_2 \quad (37)$$

For a geometrically perfect plate ($q_{10} = 0$), the initial postbuckling coefficients at elastic buckling (eigenvalue) can also be expressed by the form of Eq. (36). However, the A coefficient has to be derived from Eqs. (34) and (35) and for this case it is found to be

$$A \equiv 3(3 - \nu^2)(k_1^2 + k_2^2) + 12\nu k_1 k_2 \quad (38)$$

Eq. (36) with this A (Eq. (38)) shows that the initial postbuckling stiffness of geometrically perfect plates is constant for a given mode shape. Further, comparison with Eq. (37) shows that its value is identical to the initial stiffness, at zero loading, of plates with large imperfections ($q_{10} \gg 1$).

As a special reference case, the pure uniaxially loaded plate is considered. Its postbuckling behaviour is derived by ensuring the perpendicular incremental stress to be zero, i.e.

$$\Delta\sigma_2 = 0 \quad (39)$$

Eq. (33) is then reduced to the incremental postbuckling stiffness relation given by

$$\Delta\sigma_1 = C_{\text{uni}} \Delta\varepsilon_1 \quad (40)$$

where

$$C_{\text{uni}} = C_{11} - \frac{(C_{12})^2}{C_{22}} \quad (41)$$

Another special case is the square plate buckling into a $m = 1$ and $n = 1$ mode. For this case, the analytical, closed-form stiffness coefficients $C_{\alpha\beta}$ in Eq. (36) take on the simplest forms, given by

$$\begin{aligned} C_{11} &= \frac{2E}{(1+\nu)(3-\nu)} \\ C_{12} &= -\frac{(1-\nu)E}{(1+\nu)(3-\nu)} = C_{21} \\ C_{22} &= \frac{2E}{(1+\nu)(3-\nu)} = C_{11} \end{aligned} \quad (42)$$

By comparing Eq. (42) with the corresponding first terms in Eq. (18), that represents the unbuckled plate, it can be shown that the axial postbuckling stiffness C_{11} is only 52% of that of an unbuckled plate with a Poisson number of 0.3. The coefficient C_{12} , for the Poisson coupling effect, has changed sign and has a value of -61% of that of the unbuckled plate.

For pure axial compression, Eqs. (39) and (40) give the well-known result

$$C_{\text{uni}} = \frac{E}{2} \quad (43)$$

Eq. (42) can alternatively in this case be written as

$$\begin{aligned} C_{11} &= \frac{E^*}{1-(\nu^*)^2} \\ C_{12} &= \frac{E^*\nu^*}{1-(\nu^*)^2} = C_{21} \\ C_{22} &= \frac{E^*}{1-(\nu^*)^2} \end{aligned} \quad (44)$$

Except for the superscript, this is the exact same form as that of the stiffness coefficients of a plane stress, isotropic material. The elastic, isotropic material constant E and ν are above replaced by the modified material constants E^* and ν^* defined

as

$$\begin{aligned} E^* &= \frac{1}{2}E \\ \nu^* &= -\frac{1}{2}(1-\nu) \end{aligned} \quad (45)$$

These E^* and ν^* constants are not physical in nature like E and ν . Rather, they are mathematical, or “conceptual” in nature. In the latter sense they are fictitious material properties, but very convenient in the behavioural description.

From these simple expressions, it can be concluded that an elastically buckled square plate has in-plane stiffness properties that are equal to those of an elastic isotropic material with a modified modulus of elasticity of 50% of Young’s modulus and with a modified negative Poisson effect equal to -0.35 for a material with $\nu = 0.3$.

The directional stiffness parameter defined in Eq. (9) is especially interesting since it provides information about the stiffness change along the load history path for combined loads. As examples, cases with strain (plate-shortening) control of a square plate are considered below. For easy interpretation, the results are given as ratios of the directional postbuckling stiffness and the directional prebuckling stiffness (for standard linear elastic plane stress conditions).

Uniaxial plate-shortening control $d = 0$ (angle d is measured from the positive ε_1 strain axis):

$$\frac{C_{1\text{post}}^0}{C_{1\text{pre}}^0} = \frac{2(1-\nu)}{(3-\nu)} \approx 0.52 \quad (\nu = 0.3) \quad (46a)$$

$$\frac{C_{2\text{post}}^0}{C_{2\text{pre}}^0} = -\frac{(1-\nu)^2}{(3-\nu)\nu} \approx -0.61 \quad (\nu = 0.3) \quad (46b)$$

Balanced (equal) biaxial compressive strains; $d = 45$ degrees:

$$\frac{C_{1\text{post}}^{45}}{C_{1\text{pre}}^{45}} = \frac{(1-\nu)}{(3-\nu)} \approx 0.26 \quad (\nu = 0.3) \quad (47)$$

Comparison of Eq. (46a) and (47) shows that balanced biaxial loading reduces the postbuckling stiffness below that of uniaxially strained plates by as much as 50%. This result is identical to results published by Budiansky [3] for proportional load control of a square plate.

For the standard reference case of uniaxial stress (not shortening), the angle d for the proportional load history is $d = -16.7$ degrees up to elastic buckling. The postbuckling stiffness ratio for this case takes the classical value

$$\frac{C_{1\text{post}}^{-16.7}}{C_{1\text{pre}}^{-16.7}} = \frac{1}{2} = 0.5 \quad (48)$$

4. Multi-degree-of-freedom-model (MDOF)

Multi-degrees-of-freedom-models for both unstiffened and stiffened rectangular plates have previously been presented and

given a detailed treatment in [15–18]. Here, only some basic equations relevant for the present study, and mostly related to the transformation from load control to plate-shortening control, are given some explanations.

The same plate theory described in Section 3.1 is used, but the buckling mode and the imperfection field description are extended to multi-degrees-of-freedom using double Fourier expansions defined by

$$w = q_i h_i(x_1, x_2) = \sum_{m=1}^M \sum_{n=1}^N A_{mn} \sin\left(\frac{m\pi}{a}x_1\right) \times \sin\left(\frac{n\pi}{b}x_2\right) \quad (49)$$

$$w_0 = q_{i0} h_i(x_1, x_2) = \sum_{m=1}^M \sum_{n=1}^N A_{mn}^0 \sin\left(\frac{m\pi}{a}x_1\right) \times \sin\left(\frac{n\pi}{b}x_2\right) \quad i = 1, 2, \dots, K$$

Here the q_i is a short form notation for the Fourier amplitudes A_{mn} and h_i represent the corresponding global Fourier function ($q_1 = A_{11}/t, q_2 = A_{12}/t, \dots, q_K = A_{MN}/t$). $K = M^*N$ is the total number of degrees of freedom. The summation convention is used whenever appropriate.

As for the SDOF model, the MDOF model is developed for straight in-plane plate edges.

Substitution of Eq. (49) into Eq. (19), and also using the membrane stress distribution as given in [17], give a set K of nonlinear equilibrium equations that generally are written as

$$f_i(q_1, q_2, \dots, q_K, \sigma_1, \sigma_2) = 0 \quad i = 1, 2, \dots, K \quad (50)$$

These equations are explicit in the independent set of biaxial loads (σ_1, σ_2) and are thus suitable for load control analyses. However, they may be rewritten in a form suitable for shortening control by using the multi-degree equivalent of Eq. (18), which may be written

$$\sigma_1 = \frac{E}{1-\nu^2}(\varepsilon_1 + \nu\varepsilon_2) - \frac{\pi^2}{8} \frac{E}{1-\nu^2}(c_1 + \nu c_2) \quad (51)$$

$$\sigma_2 = \frac{E}{1-\nu^2}(\varepsilon_2 + \nu\varepsilon_1) - \frac{\pi^2}{8} \frac{E}{1-\nu^2}(c_2 + \nu c_1)$$

where the coefficients c_1 and c_2 are defined by

$$c_1 = \frac{1}{a^2} \sum_{m=1}^M \sum_{n=1}^N m^2 (A_{mn}^2 + 2A_{mn}A_{mn}^0) \quad (52)$$

$$c_2 = \frac{1}{b^2} \sum_{m=1}^M \sum_{n=1}^N n^2 (A_{mn}^2 + 2A_{mn}A_{mn}^0)$$

Then, by substituting Eq. (51) into (50), the equilibrium equations are transformed to a set of equations

$$f_i(q_1, q_2, \dots, q_K, \varepsilon_1, \varepsilon_2) = 0 \quad i = 1, 2, \dots, K \quad (53)$$

suitable for plate-shortening control analyses specified as load-histories in strain (plate-shortening) space.

An arbitrarily curved and continuous load history in load or strain space, spanned by two independent load parameters Λ_1

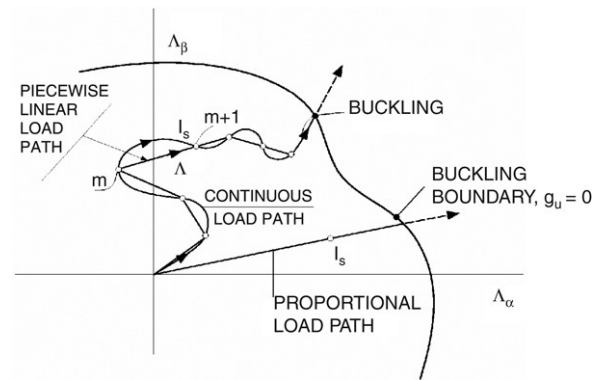


Fig. 3. Schematic illustration of continuous (“piecewise linear”) and proportional loading sequence in load or strain (plate-shortening) space.

and Λ_2 , can be described by a piecewise linear curve through a set of L specified points, or load stages, $\Lambda_{1,m}$ and $\Lambda_{2,m}$ ($m = 1, 2, 3, \dots, L$), as illustrated schematically in Fig. 3. Along each piecewise linear step, between load stages, the load history is described by

$$\Lambda_1 = \Lambda_{1,m} + \Lambda(\Lambda_{1,m+1} - \Lambda_{1,m}) \quad (54)$$

$$\Lambda_2 = \Lambda_{2,m} + \Lambda(\Lambda_{2,m+1} - \Lambda_{2,m})$$

Here Λ is a single load multiplier taking prescribed values between zero and unity for each linear step along the specified load path. Including the zero load state, a proportional loading path definition needs only two reference points in load space, i.e. Eq. (54) simplifies to

$$\Lambda_1 = \Lambda \Lambda_{1,1} \quad (55)$$

$$\Lambda_2 = \Lambda \Lambda_{2,1}$$

In addition to the general load path, Fig. 3 also includes a proportional path. Later example computations will be restricted to proportional paths.

With the chosen division of the load history into load stages, Λ is the only load parameter in each linear load step from one stage to another. Thus, the equilibrium equations, Eqs. (50) and (53) can be written as

$$f_i(q_1, q_2, \dots, q_K, \Lambda) = 0 \quad i = 1, 2, \dots, K \quad (56)$$

Using the perturbation method, a solution of Eq. (56) is sought in the form of a Taylor expansion around a known state (state s indicated as superscript) in terms of a continuously increasing perturbation parameter η along the equilibrium path. This gives

$$q_i = q_i(\eta) = q_i^s + \dot{q}_i^s \Delta\eta + \frac{1}{2!} \ddot{q}_i^s (\Delta\eta)^2 + \dots \quad (57)$$

$$\Lambda = \Lambda(\eta) = \Lambda^s + \dot{\Lambda}^s \Delta\eta + \frac{1}{2!} \ddot{\Lambda}^s (\Delta\eta)^2 + \dots$$

for the deflection parameters and the load multiplier. A dot (above a parameter) indicates differentiation with respect to η .

In order to ensure an always increasing perturbation parameter along the equilibrium path, the arc length along the curve becomes the obvious choice for η . The arc length

parameter is defined by

$$\eta - \eta^s = \dot{q}_i^s (q_i - q_i^s) + \dot{\Lambda}^s (\Lambda - \Lambda^s) \quad (58)$$

By differentiating once with respect to η , the equilibrium equation, Eq. (56), and the load incrementation equation, Eq. (58), can be written on first-order rate form as

$$f_i^j \dot{q}_j + f_i^A \dot{\Lambda} = 0 \quad i, j = 1, \dots, K \quad (59a)$$

$$\dot{q}_i \dot{q}_i + \dot{\Lambda}^2 = 1 \quad i = 1, \dots, K \quad (59b)$$

where superscripts j and A indicate partial differentiation with respect to the deflection parameter q_j and the load parameter Λ , respectively. The superscript s have been deleted for convenience. From the K linear equations of Eq. (59a), the K unknown deflection rates can be solved for in terms of the unknown load rate parameter $\dot{\Lambda}$, which, finally, can be determined from Eq. (59b). For additional details, reference is made to [13,17].

In matrix notation, Eq. (59a) is written as

$$\mathbf{K}\dot{\mathbf{A}} - \mathbf{G}\dot{\Lambda} = \mathbf{0} \quad (60)$$

\mathbf{K} is the incremental stiffness matrix, $\dot{\mathbf{A}}$ is the displacement rate vector and $\mathbf{G}\dot{\Lambda}$ is the incremental load vector. In a similar manner, it is straightforward to derive the second-order equations for finding the path derivatives in the Taylor expansion, Eq. (57). The resulting equations, obtained by differentiating Eq. (59) once with respect to η can be given in the form

$$\mathbf{K}\ddot{\mathbf{A}} + \mathbf{H}\ddot{\Lambda} = \mathbf{0} \quad (61a)$$

$$\dot{q}_i \ddot{q}_i + \dot{\Lambda} \ddot{\Lambda} = 0 \quad i, j = 1, \dots, K \quad (61b)$$

However, the solution for second-order path derivatives is not pursued here. The incrementation strategy adopted is to use first-order path derivatives only, but in combination with incremental $\Delta\eta$ values that are sufficiently small, so as to provide results with satisfactory accuracy without having to make equilibrium controls, and corrections. In comparison, Riks' arc length method [30], which in many respects is similar to the present approach, requires equilibrium controls to be made. It has been found, in numerous comparisons, that incremental $\Delta\eta$ values in the order of 0.01 to 0.02 provide very accurate tracing of the equilibrium path.

5. Case study — postbuckling stiffness results

Closed-form, single-degree-of-freedom solutions (SDOF) are compared with corresponding analytical multi-degree-of-freedom solutions (MDOF) and with nonlinear finite element method (FEM) results obtained using a commercial FEM program [21]. Linear elastic, plane stress conditions are used in all computations.

One specific rectangular plate geometry is analysed for five different proportional load histories in strain space $(\varepsilon_1, \varepsilon_2)$. Results are presented in terms of corresponding load paths mapped into the load space (σ_1, σ_2) and as load-shortening curves in spaces $(\sigma_i, \varepsilon_1, \varepsilon_2)$. The load paths mapped into load

space (σ_1, σ_2) are convenient for illustrating how the biaxial load redistribution has to take place in order to keep the plate in equilibrium under prescribed plate shortenings. The load-shortening curves, on the other hand, effectively show how the in-plane stiffness changes for each load component when the elastic buckling limit is exceeded and the plate is in the postbuckling region.

The geometrical imperfection shape (w_0) is taken identical to the “minimum eigenmode”, i.e. the buckling mode corresponding to the lowest eigenvalue and with an imperfection amplitude of 1% of the plate thickness. This small imperfection, representative for nearly perfect plates, was set in order to trace the largest stiffness change a plate can experience. Note that the MDOF model in the examples always has a full range of half-waves $m = 1, 2, 3, \dots; n = 1, 2, 3 \dots$ for describing the postbuckling deflection pattern even though the imperfection shape is only defined with one simple sinusoidal wave (one term in Fourier series always).

Complex and randomly distributed imperfection patterns, as present in real welded structures, can cause a different postbuckling response than that in the perfect case, especially if the imperfections are large in amplitude. However, to study mode snapping and interactive nonlinear behaviour in geometrically imperfect plates was not the main purpose of the present work and thus that topic has only been given minor attention in the following discussions.

The ABAQUS plate models are meshed with square shaped, four node elements with reduced integration (type S4R). Experience shows that six elements across the shortest plate edge gives sufficient accuracy and is used in the present study. The nodes along each plate edges are forced to remain on a straight line in-plane and relative plate shortenings are prescribed as proportional load rays in strain space $(\varepsilon_1, \varepsilon_2)$. For out-of-plane effects, classical simply supported boundary conditions are assumed along all edges, i.e. edges are free to rotate while restrained to remain in the plate plane.

The rectangular example plate has the following properties: $a = 3000$ mm, $b = 1000$ mm, $t = 17$ mm, $E = 210\,000$ N/mm², Poisson $\nu = 0.3$, Imperfection amplitude = 0.17 mm in the minimum eigenmode. $\sigma_F = 315$ N/mm² (σ_F is the yield stress used for scaling purposes only of the axes in the following figures. It does influence the nonlinear geometrical results as shown)

The five different proportional strain paths considered are shown in Fig. 4 and defined by the angle d measured between the positive ε_1 -axis and the proportional path. The five angles analysed are $d = -16.7, 0, 45, 90, 106.7$ degrees.

When analysing rectangular plates, it is important to focus on more modes than just the minimum eigenmode and also on the fact that the shape of minimum eigenmode may be different for different load combinations.

Fig. 4, shows eigenvalue boundaries for 4 modes defined by $(m = 1, n = 1)$, $(m = 2, n = 1)$, $(m = 3, n = 1)$, $(m = 4, n = 1)$. For all load histories analysed the minimum eigenmode has one half-wave across the plate width b . Thus only the $n = 1$ modes are illustrated in Fig. 4.

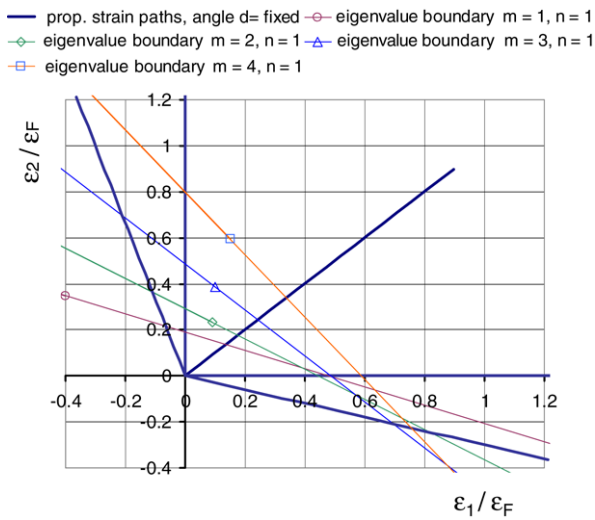


Fig. 4. Specified proportional load histories in biaxial strain space and eigenvalue boundaries for a rectangular plate: $a = 3000$ mm, $b = 1000$ mm, $t = 17$ mm. The five prop. strain paths have angles d with positive ε_2 -axis: $d = -16.7, 0, 45, 90, 106.7$ degrees.

From these eigenvalue boundary results it can be observed that for almost the whole biaxial compression zone, particularly the region for which the transverse shortening ε_2 is dominating, the critical eigenmode will correspond to a long waded mode ($m = 1, n = 1$). When a plate is compressed beyond this eigenvalue boundary, the deflected form will flatten out in the mid-region and the plate will typically have a postbuckled “hungry horse” shape, as illustrated in Fig. 5(a). For plates with dominating axial shortening ε_1 , Fig. 4 shows that the eigenvalues for different buckling modes are clustered together. This is thus a region where mode snapping is likely to occur, as discussed further below.

The five different proportional strain paths in Fig. 4 are mapped into load space in Fig. 6. For each load path the imperfection shape is taken equal to the minimum eigenmode. The four lowest eigenvalue boundaries are also shown in the figure. They are given by straight lines and are useful for illustration of the connections between the elastic buckling limits and the load level at which the biaxial load redistributions take place.

Each of the load paths can be seen to exhibit a clear bend when passing the eigenvalue boundary. This indicates that significant biaxial load redistributions have to take place in order to keep the plate in equilibrium for forced proportional plate shortenings.

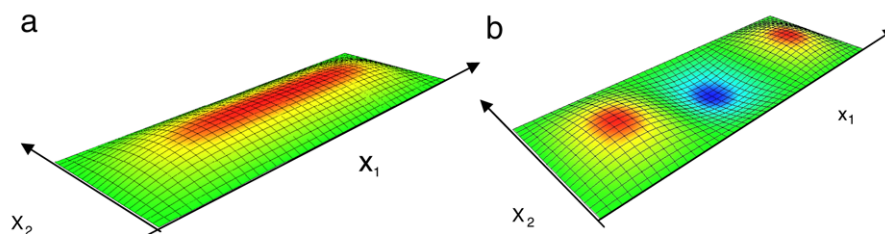


Fig. 5. Postbuckled rectangular plates; (a) transversely dominating compression, (b) longitudinally dominating compression.

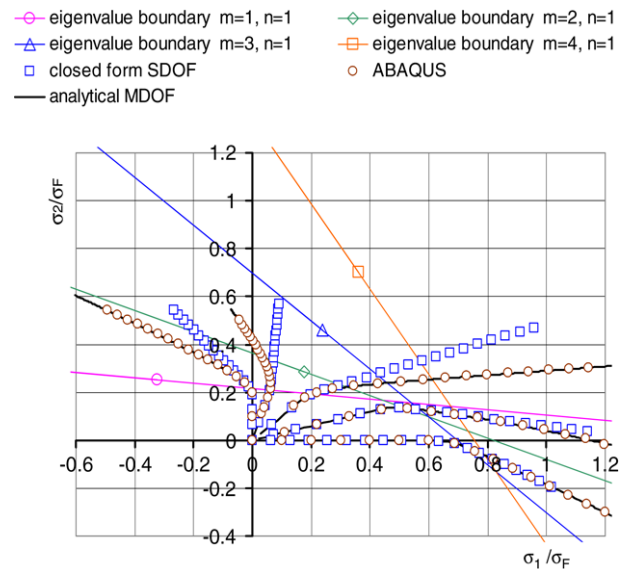


Fig. 6. Five calculated load paths in biaxial load space and eigenvalue boundaries for a rectangular plate: $a = 3000$ mm, $b = 1000$ mm, $t = 17$ mm. Curves are valid for small geometrical imperfections (0.17 mm in the minimum eigenmode). The five load paths corresponding to $d = -16.7, 0, 45, 90$ and 106.7 degrees are shown as curves emanating from the origin. The $d = -16.7$ case starts along the σ_1 -axis, with the other paths found in the anticlockwise direction.

It can also be seen (Fig. 6) that the closed-form solution resembles the numerical solutions in cases when axial load (σ_1) dominates while it diverges significantly from the numerical solutions in cases with dominating transverse load (σ_2). Moreover, it is seen that the analytical MDOF solution and the ABAQUS solutions almost coincide for all cases.

In the following, results for each of the five load paths are discussed separately.

$d = -16.7$ degrees. The prebuckling load path for this case follows the abscissa (σ_2 -axis) in Fig. 6 for then to bend down beyond the minimum eigenvalue boundary in mode $m = 3$. The axial load continues to increase while the transverse stress starts unloading and becomes negative (tension). Fig. 7 shows the corresponding load-shortening curves indicating an axial stiffness drop in the order of 45% when loaded beyond elastic buckling. The postbuckling response curves are also very close to being linear, indicating that the eigenmode shape is well maintained in the postbuckling region. This is also the reason for the good correlation in this case with the closed-form solution, which assumes that the displacement shape in the postbuckling region is equal to that of the eigenmode.

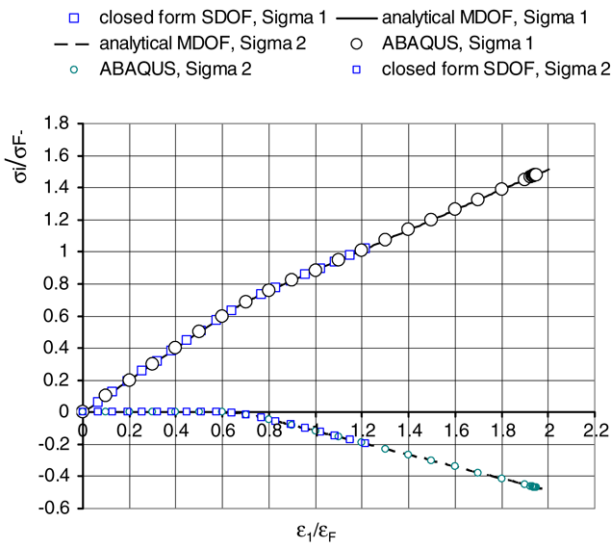


Fig. 7. Calculated load-shortening curves valid for proportional strain path $d = -16.7$ degrees. Rectangular plate: $a = 3000$ mm, $b = 1000$ mm, $t = 17$ mm. Curves are valid for small geometrical imperfections (0.17 mm in the minimum eigenmode $m = 3, n = 1$).

It is seen that, for all practical purposes, the closed-form SDOF, the analytical MDOF and the ABAQUS results are coincident.

$d = 0$ degrees ($\varepsilon_2 = 0$). In this case, the three first eigenvalues are clustered close together (Fig. 4), with the minimum value obtained for $m = 2$. The next two eigenvalues, for $m = 1$ and $m = 3$, are almost identical and only slightly greater than the minimum value. Due to the cluster of eigenvalues, this case is therefore analysed for an imperfection in shape $m = 2$ and shape $m = 3$ respectively.

Again, Fig. 6 shows the significant biaxial load redistribution that takes place when passing the minimum eigenvalue. In the postbuckling region, the axial load continues to increase while the transverse load decreases. Fig. 8 shows the corresponding non-dimensional load-shortening curves for σ_1 and σ_2 vs. ε_1 . Also, in addition to the standard case with the initial imperfection taken in the shape of the lowest buckling mode ($m = 2$), the figure also includes results computed with the initial imperfection taken equal to the higher mode $m = 3$. The reason for this also including the latter case is that it has an eigenvalue only slightly higher than the minimum value for $m = 2$ and that in such cases snapping from one mode to another may occur.

The figure clearly shows that the higher $m = 3$ mode imperfection causes a smaller axial postbuckling stiffness than does the lowest ($m = 2$) one. This is in contrast to the normal assumption that the use of imperfections in the shape of the minimum eigenmode is conservative. The axial stiffness in the $m = 3$ mode is in the order of 25% less than that in the $m = 2$ mode. This is a significant difference. Also for these cases, the load-shortening responses are close to being linear curves in the postbuckling range shown. In the advanced postbuckling range, the buckled shape in the initial $m = 2$ mode tends to flatten out as contributions from the $m = 3$ mode slowly starts growing.

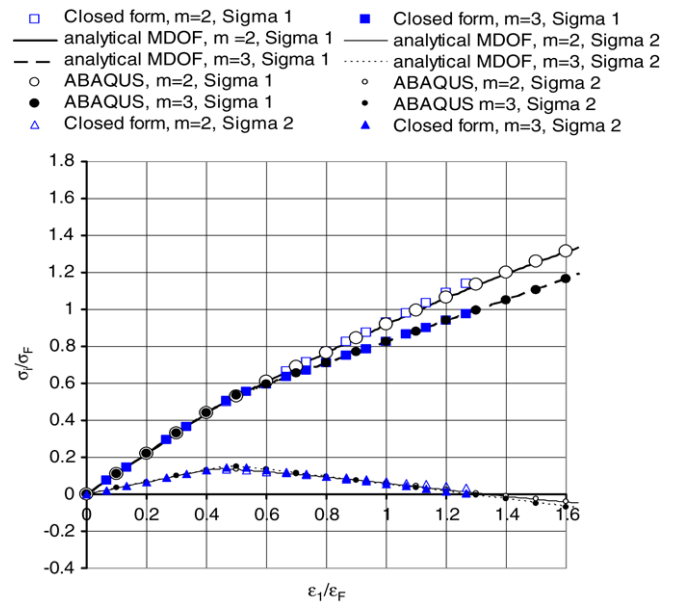


Fig. 8. Calculated load-shortening curves valid for proportional strain path $d = 0$ degrees. Rectangular plate: $a = 3000$ mm, $b = 1000$ mm, $t = 17$ mm. Curves are valid for small geometrical imperfections (0.17 mm in the eigenmodes $m = 2$ and $m = 3$).

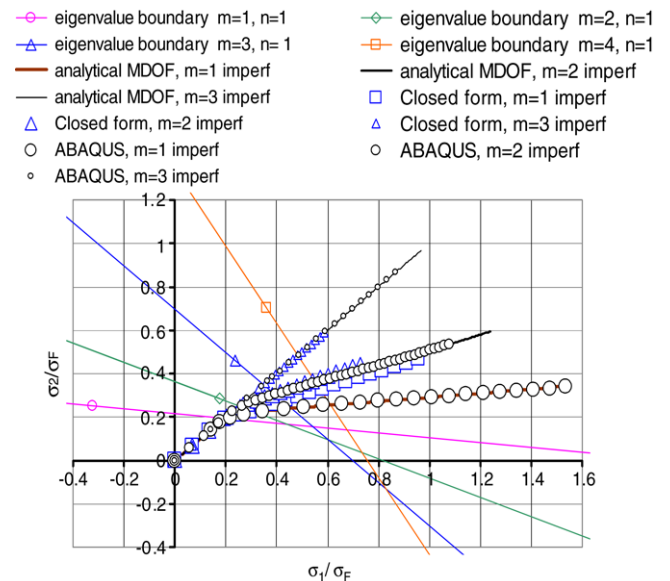


Fig. 9. Calculated load paths in biaxial load space for balanced proportional plate shortening $d = 45$ degrees for a rectangular plate: $a = 3000$ mm, $b = 1000$ mm, $t = 17$ mm. Curves are valid for small geometrical imperfections (0.17 mm) in the eigenmodes $m = 1, m = 2$ and $m = 3$ individually.

Finally, snapping to a pure $m = 3$ postbuckling mode takes place far beyond the load range shown in Fig. 8.

It is seen that, for all practical purposes, the closed form, the analytical MDOF and the ABAQUS results are coincident.

$d = 45$ degrees. The load path results for this case, Fig. 6, calculated with an imperfection shape in the form of the minimum eigenmode ($m = 1$, Fig. 4), show a significant difference between the MDOF and ABAQUS solution on the one side and the closed-form solution on the other. In order

to study the reason for this differences in more detail, results for the different geometrical imperfections modes, defined by $m = 1$ and the higher $m = 2$ and $m = 3$ modes, are shown in load space, Fig. 9.

It is observed in Fig. 9 that the biaxial load redistribution is less for higher imperfection modes than that for the $m = 1$ mode and with the $m = 3$ mode giving no biaxial load redistribution. This is natural since the $m = 3$ buckling mode for a rectangular plate of aspect ratio 3 ($a/b = 3$) gives a square deflection mode shape. Balanced biaxially 50%–50% ($d = 45$ degrees) compression on a square local plate buckle gives naturally no biaxial load shedding. However, in practice all welded steel plates will have a significant $m = 1$ imperfection mode contribution with minor components in higher modes. For such plates the present nonlinear analyses show that the $m = 1$ mode will dominate the response with a deflection pattern shown in Fig. 5(a) as typical for the postbuckling region. This deflection mode, with a flattened shape in the mid-regions gives low membrane stiffness in the transverse direction, explaining the marginal increase in the transverse load and the significant increase in the axial load.

Fig. 10 shows the load-shortening curves for $d = 45$ assuming geometrical imperfections in the minimum eigenmode $m = 1$ only. It can be once more concluded that the plate stiffness changes radically beyond elastic buckling limit, and particularly the stiffness against transverse loading is almost non-existing in the postbuckling region. For this example, with plate thickness 17 mm, the plate will buckle elastically at approximately 20% of the material yield stress. Due to the very low transverse stiffness beyond the elastic buckling limit, the transverse stress will only increase marginally for increasing prescribed plate shortenings. The postbuckling stiffness curves are no longer linear, but tend to be somewhat nonlinear with a slight drop in stiffness far into the postbuckling region.

As observed, the analytical MDOF solution and ABAQUS give almost identical results while the closed-form solution predicts too stiff load-shortening responses.

$d = 90$ degrees ($\varepsilon_1 = 0$). As before, the sharp bend in the axial load curve (σ_1) in Fig. 6 illustrates a significant biaxial load redistribution when passing the minimum eigenmode $m = 1$. However, in this case it is associated with a continuous increase in transverse load and an unloading in the axial load from compression to tension when the plate is shortened transversely (ε_2) far into the postbuckling region. Fig. 11 shows the corresponding load-shortening curves assuming geometrical imperfections in the minimum eigenmode $m = 1$ only.

The interesting observation is the radical loss of stiffness in the transverse load σ_2 direction and the change to negative stiffness in the axial load direction. The loss of transverse stiffness is typically more than 80% compared to stiffness of the unbuckled plate.

It is also observed that the analytical MDOF solution and ABAQUS gives almost identical results while the closed-form solution predicts a somewhat too stiff load-shortening response.

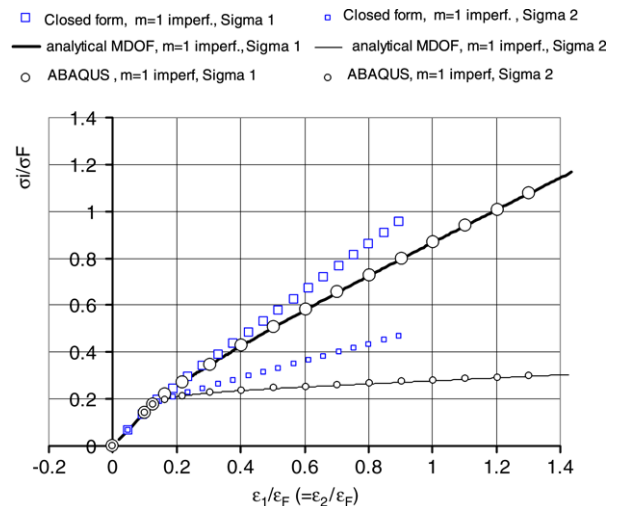


Fig. 10. Calculated load-shortening curves valid for proportional strain path $d = 45$ degrees. Rectangular plate: $a = 3000$ mm, $b = 1000$ mm, $t = 17$ mm. Curves are valid for small geometrical imperfections (0.17 mm) in the minimum eigenmode $m = 1$.

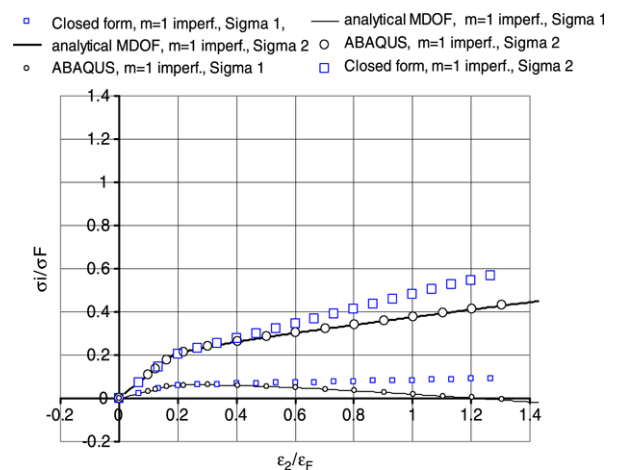


Fig. 11. Calculated load-shortening curves for proportional strain path $d = 90$ degrees. Rectangular plate: $a = 3000$ mm, $b = 1000$ mm, $t = 17$ mm. Curves are valid for small geometrical imperfections (0.17 mm) in the minimum eigenmode $m = 1$.

$d = 106.7$ degrees. Fig. 6 shows a significant biaxial load redistribution with the continuously increasing transverse load while an axial tension load built up in the longitudinal direction.

Fig. 12 shows the corresponding load-shortening curves assuming geometrical imperfections in the minimum eigenmode $m = 1$ only. As for the $d = 90$ degree case, the interesting observation is the radical loss of stiffness for the transverse load σ_2 beyond the eigenvalue boundary. The loss of stiffness is typically more than 70% compared to an unbuckled plate solution.

Again, it is observed that the analytical MDOF solution and ABAQUS give almost identical results while the closed-form solution predicts somewhat too stiff load-shortening responses.

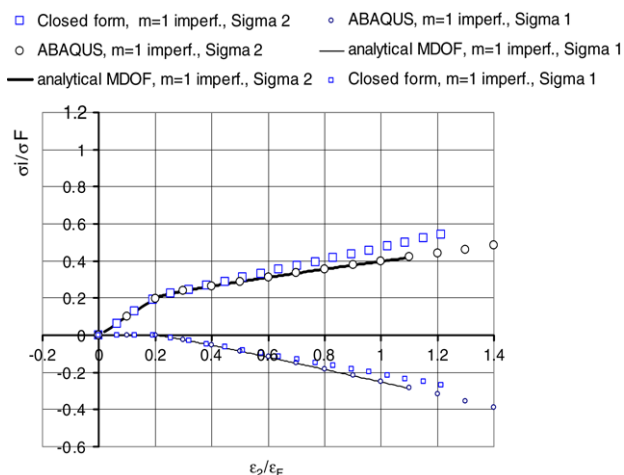


Fig. 12. Calculated load-shortening curves for proportional strain path $d = 106.7$ degrees. Rectangular plate: $a = 3000$ mm, $b = 1000$ mm, $t = 17$ mm. Curves are valid for small geometrical imperfections (0.17 mm) in the minimum eigenmode $m = 1$.

6. Conclusions

An analytical closed-form solution and a more advanced analytical MDOF plate model are developed in a form suited for studying the biaxial load redistribution and change of in-plane stiffness (membrane) behaviour of elastically buckled plates. A specific example is analysed in detail and the results from the analytical models are validated against nonlinear finite element results obtained using the computer program ABAQUS [21].

The comparisons show that the developed analytical MDOF model gives almost identical results to the ABAQUS analyses over the whole range of example parameters. The closed-form solution (SDOF) shows good correlation with the other two solutions as long as the deflection shape is relatively short waved as typical for low aspect ratio plates ($a/b \leq 2$) or axially dominated loading on long rectangular plates.

The results presented, and the structural response observed, highlight stiffness changes and load shedding properties of elastically buckled plates compressed biaxially under plate-shortening control. It is shown that significant load redistribution takes place under a prescribed biaxial plate-shortening ratio as typical for plate elements being a part of larger plate structures. This leads to very different stress levels in the plate as compared to results from linear analysis used in normal ship design procedures.

Technically, the biaxial load shedding properties of elastically buckled plates signify the importance of including all relevant coupling terms in simplified macro-material formulations used for linear as well as nonlinear global strength assessments of ships etc. Moreover, it is also shown that the lowest postbuckling stiffness is not always associated with the minimum eigenvalue mode, a feature which is important to consider for lower bound strength assessments.

The MDOF model presented herein is implemented into the computerized buckling code PULS developed by Det Norske Veritas [19].

Acknowledgements

We would like to thank our colleagues B. Cerup-Simonsen, G. Holtmark, S. Valsgård, T.K. Østvold, K.G. Vilming, Å. Bøe, Lars Brubak, Jon Kippenes all at DNV, for their continuous technical support, and to DNV for financial support. Appreciations also goes to prof. O. Hughes, Virginia Tech State University, U.S., for his interest in the present work.

References

- [1] Koiter WT. On the stability of elastic equilibrium (in Dutch with English summary). Thesis, Delft, H.J. Paris, Amsterdam. English translation: Air Force Flight Dyn. Lab. Tech. Rep. AFFDL-TR-70-25, Stanford University, Dept. of Aeronautics and Astronautics, USA, 1970, 1945.
- [2] Koiter WT. Introduction to the post-buckling behaviour of flat plates. *Memoires in -8° de la Societe Royale des Sciences de Liege*, 5^{ième} serie, Tome VIII, Fascicule 5. 1963; p.17–40.
- [3] Budiansky B. Theory of buckling and post-buckling behaviour of elastic structures. *Advances in applied mechanics*, vol. 14. Academic Press; 1974.
- [4] Tvergaard V. Imperfection sensitivity of a wide integrally stiffened panel under compression. *Int J Solids Struct* 1973;9:177–92.
- [5] Walker AC. Interactive buckling of structural components. *Sci Progr* 1975;62:579–97.
- [6] Ueda Y, Yao T. The influence of complex initial deflection modes on the behaviour and ultimate strength of rectangular plates in compression. *Int J Struct Eng* 1978;56A.
- [7] Rhodes J. Effective widths in plate buckling. In: Rhodes J, Walker AC, editors. *Developments in thin-walled structures-1*. London: Applied Science Publishers; 1982.
- [8] Paik JK, Thayamballi AK, Wang G, Kim BJ. On Advanced Buckling and Ultimate Strength Design of Ship Plating. In: *SNAME annual meeting 2000*.
- [9] Steen E, Østvold TK, Valsgård S. A new design model for ultimate and buckling strength assessment of stiffened plates. *PRADS 2001*, 2001.
- [10] Steen E, Byklum E, Vilming KG, Østvold TKS. Computer efficient non-linear buckling models for capacity assessment of stiffened panels subjected to combined loads. In: *ICTWS 2004, fourth international conference on thin-walled structures*. UK: Loughborough University; 2004.
- [11] Steen E, Byklum E, Vilming KG, Østvold TKS. Computerized buckling models for ultimate strength assessment of stiffened ship hull panels. In: *PRADS 2004*. 2004.
- [12] Steen E. Elastic buckling and postbuckling of eccentrically stiffened plates. *Int J Solids Struct* 1989;25(7):751–68.
- [13] Steen E. Application of the Perturbation Method to Plate Buckling Problems. *Research report in mechanics*, No. 98-1. Norway: Mechanics Division, Department of Mathematics, University of Oslo; 1998.
- [14] Steen E. Buckling of stiffened plates using a Shanley model approach. *Research report in mechanics*, No. 99-1. Norway: Mechanics Division, Department of Mathematics, University of Oslo; 1999.
- [15] Byklum E, Amdahl J. Nonlinear buckling analysis and ultimate strength prediction of stiffened steel and aluminium panels. In: *The second int. conference on advances in structural engineering and mechanics*. 2002.
- [16] Byklum E, Amdahl J. A simplified method for elastic large deflection analysis of plates and stiffened panels due to local buckling. *Thin-Walled Struct* 2002;40:923–51.
- [17] Byklum E. Ultimate strength analysis of stiffened steel and aluminium panels using semi-analytical methods. Ph.D thesis. Trondheim, Norway: Norwegian University of Science and Technology; 2002.
- [18] Byklum E, Steen E, Amdahl J. A semi-analytical model for global buckling and postbuckling analysis of stiffened panels. *Thin-Walled Struct* 2004;42:701–17.
- [19] Det Norske Veritas (2004) Report no. 2004-0406. PULS 2.0 – User's manual'.

- [20] Det Norske Veritas (2002). Recommended Practice C201. Buckling Strength of Plated Structures, October 2002.
- [21] ABAQUS (2005). Version 6.5, User's manual. USA: Hibbitt, Karlsson & Sorensen, Inc.; 2005.
- [22] Hughes O. Ship structural design, a rationally-based, computer-aided optimization approach. New Jersey: SNAME; 1988.
- [23] Fujikubo M, Yao T. Elastic local buckling strength of stiffened plates considering plate/stiffener interaction and welding residual stress. *Marine Struct* 1999;12:543–64.
- [24] Ishibashi K, Fujikubo M, Yao T. Development of ISUM element for rectangular plate with cutout. In: Proceedings of the sixteenth international offshore and polar engineering conference. 2006.
- [25] Paik JK, Thayamballi AK. Ultimate limit state design of steel-plated structures. Chichester (UK): John Wiley & Sons; 2003.
- [26] Washizu K. Variational methods in elasticity and plasticity. 2nd ed. Bath (Great Britain): Pergamon Press; 1975.
- [27] Marguerre K. Zur theorie der gekrümmten platte grosser formeändrug. In: Proceedings of the 5th international congress for applied mechanics. 1938 p. 93–101.
- [28] Brush DO, Almroth BO. Buckling of bars, plates, and shells. International student edition. McGraw-Hill; 1975.
- [29] Hutchinson JW, Koiter WT. Postbuckling theory. *Appl Mech Rev* 1970; 23.
- [30] Riks E. An incremental approach to the solution of snapping and buckling problems. *Int J Solids Struct* 1979;15:529–51.